Journal of Mathematical Chemistry 23 (1998) 327–351

On the extension of quantum similarity to atomic nuclei: Nuclear quantum similarity

David Robert and Ramon Carbó-Dorca

Institute of Computational Chemistry, University of Girona, 17071 Girona, Catalonia, Spain

Received 12 June 1997

Quantum similarity is a useful tool to establish comparisons between elements of a quantum object set and, so far applied successfully to molecular physics, is applied here to atomic nuclei. Quantum Similarity Measures (QSM) and Indices (QSI) are introduced to study an arbitrary set of 20 nuclei. From this study, relationships between nuclear overlap-like self-similarities and size-like properties are found. A bidimensional projection of the set is performed, and Mendeleev conjecture is invoked to predict qualitatively some nuclear ground-state properties, such as total binding energy per nucleon, nuclear radius, nuclear volume, total and partial energies, etc.

1. Introduction

Quantum Similarity (QS) is a recently developed subject [5,7,9–11,13]. It constitutes a fundamental tool to order and classify molecular systems using their density functions. However, the QS foundations are so general that it makes possible to apply it to other areas, provided that the studied systems have a quantum mechanical description. In this work, quantum similarity is applied to an arbitrary set of twenty atomic nuclei.

As a consequence of the quantum mechanical postulates, all the information which can be extracted from a quantum system is contained in its wavefunction, and in some degree, in its density function. Density function formalism may be based in the context by Löwdin and McWeeny [25–28], which states that all ground-state properties of a quantum system, and in particular the energy, can be expressed in relation to its density function.

A n-particle system (in our case, n nucleons) will be caracterized by a nth-order density function, containing all its information. Because of the evident difficulties in modelling and manipulating these functions, we will restrict our calculations to first-order density functions, assuming the derived loss of information. Thus, if two first-order density functions for two systems A and B are known, $\rho_{\mathrm{A}}(\mathbf{r}_1)$ and $\rho_{\mathrm{B}}(\mathbf{r}_2)$,

a *Quantum Similarity Measure* (QSM) can be defined as the integral

$$Z_{\mathrm{AB}} = \int_{D_1} \int_{D_2} \rho_{\mathrm{A}}(\mathbf{r}_1) \Omega(\mathbf{r}_1, \mathbf{r}_2) \rho_{\mathrm{B}}(\mathbf{r}_2) \, \mathrm{d}^3 r_1 \, \mathrm{d}^3 r_2, \tag{1}$$

where $\Omega(\mathbf{r}_1, \mathbf{r}_2)$ is a definite positive operator. A Dirac delta distribution, $\delta(\mathbf{r}_1 - \mathbf{r}_2)$, has been chosen arbitrarily here to be this operator. This transforms equation (1) into

$$Z_{\mathrm{AB}} = \int_{D} \rho_{\mathrm{A}}(\mathbf{r}) \rho_{\mathrm{B}}(\mathbf{r}) \, \mathrm{d}^3 r. \tag{2}$$

QSM derived by this way are called *overlap-like similarity measures*. In the case that density functions only have a radial dependence, this yields

$$Z_{\mathrm{AB}} = \int_{D} \rho_{\mathrm{A}}(r) \rho_{\mathrm{B}}(r) 4\pi r^2 \, \mathrm{d}r. \tag{3}$$

The integrals can be used to extract information from the set of studied quantum objects.

The results from QSM calculations can be expressed in a matrix form, where the element Z_{AB} corresponds to comparing nucleus A with nucleus B. Obviously, the QSM matrix is symmetric. Diagonal elements of this matrix are known, by obvious reasons, as *Self-Similarity Measures* (SSM).

There are various possible manipulations of QSM, called *Quantum Similarity Indices* (QSI). Among all the existing QSI, a classical one has been chosen here, the so-called Carbó Index. Using the matrix elements of the QSM, the Carbó Index is defined as

$$C_{\mathrm{AB}} = \frac{Z_{\mathrm{AB}}}{\sqrt{Z_{\mathrm{AA}} Z_{\mathrm{BB}}}}. \tag{4}$$

This index is nothing but a normalization of the similarity measures, and it can be interpreted as a generalized cosine of the angle between Hilbert space functions ρ_{A} and ρ_{B}. The Carbó Index ranges from 0 (total dissimilarity) to 1 (complete similarity), depending on the similarity measure associated to the two nuclei.

2. Nuclear density functions

Nuclear density functions have been calculated using a Hartree–Fock iterative procedure with the effective Skyrme interaction [34,40] with a SkM* parametrization [2]. More details on this model are given in appendix A.

In our study, we have chosen arbitrarily 20 nuclei along all the Periodic Table in which the Skyrme–Hartree–Fock model agrees. We have chosen a very variate set: magic, semimagic and nonmagic nuclei, stable and unstable nuclei, nuclei with integer and fractionary spin, nuclei with positive and negative parity, etc.

The set of studied nuclei is the following: ^{12}C, ^{14}N, ^{16}O, ^{28}Si, ^{35}Cl, ^{40}Ca, ^{48}Ca, ^{56}Fe, ^{56}Ni, ^{58}Ni, ^{63}Cu, ^{73}As, ^{89}Y, ^{93}Mo, ^{120}Sn, ^{124}Sn, ^{133}Cs, ^{153}Gd, ^{184}W, ^{208}Pb.

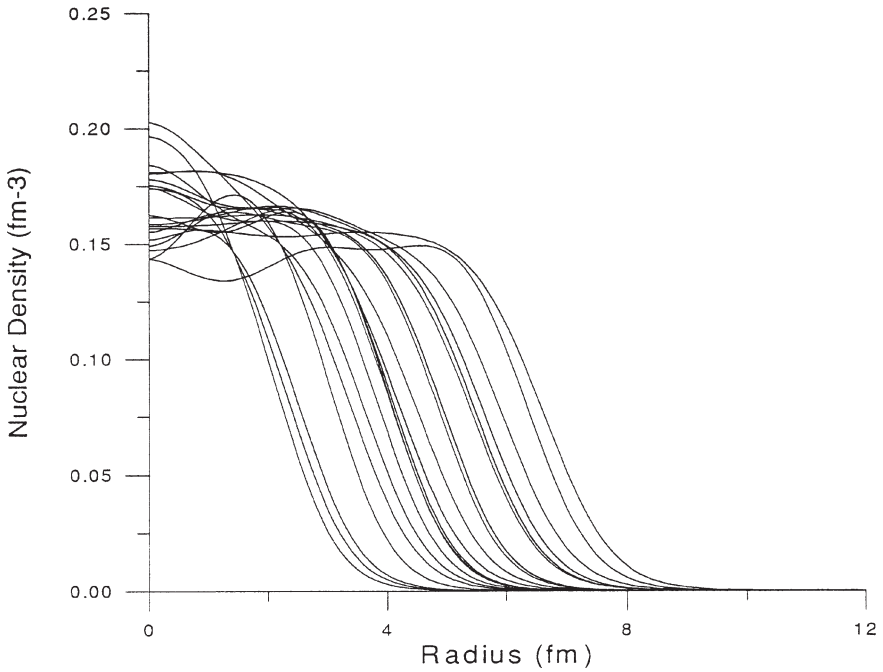

Figure 1. Skyrme–Hartree–Fock nuclear density functions (in fm^{-3}) for the twenty studied nuclei.

Numerical nuclear density functions obtained with the procedure exposed in appendix A are plotted in figure 1.

The shape of the nuclear density functions makes possible to approximate them analytically as Fermi–Dirac distributions [29,32], or as linear combinations of gaussian functions [15] or spherical Bessel functions [16], among others. In order to keep accuracy as best as possible, the numerical form will be adopted, and thus QSM integrals will be calculated numerically.

3. Results and discussion

3.1. The nuclear overlap-like self-similarity measures

QSM have been calculated numerically from definition (3), using a second-order Simpson rule [6]. QSM matrix elements are shown in table 1, and table 2 gathers the nuclear overlap-like self-similarity measures (the diagonal matrix elements Z_{AA}) for the series of 20 nuclei.

The values of table 2 show that nuclear SSM decrease from ^{208}Pb to ^{12}C. Plotting nuclear SSM versus massic number (see figure 2) one can see that self-similarities exhibit a clear linear dependence on the massic number. This relationship is more precise and simpler than the one derived for atoms, where atomic SSM were found depending on Z^3, Z being the atomic number [36].

Table 1
Quantum similarity measures matrix.

Z	^{12}C	^{14}N	^{16}O	^{28}Si	^{35}Cl	^{40}Ca	^{48}Ca	^{56}Fe	^{56}Ni	^{58}Ni	^{63}Cu	^{73}As	^{89}Y	^{93}Mo	^{120}Sn	^{124}Sn	^{133}Cs	^{153}Gd	^{184}W	^{208}Pb
^{12}C	1.0899																			
^{14}N	1.1457	1.2193																		
^{16}O	1.2044	1.2953	1.3881																	
^{28}Si	1.6189	1.7888	1.9601	2.9426																
^{35}Cl	1.7189	1.9094	2.1019	3.2268	3.6100															
^{40}Ca	1.7028	1.9138	2.1263	3.3551	3.8067	4.0662														
^{48}Ca	1.7880	2.0306	2.2747	3.6761	4.2249	4.5640	5.1737													
^{56}Fe	1.8771	2.1411	2.4067	3.9393	4.5742	4.9790	5.6844	6.2843												
^{56}Ni	1.8357	2.1051	2.3757	3.9251	4.5687	4.9873	5.7059	6.3125	6.3469											
^{58}Ni	1.8883	2.1584	2.4300	3.9965	4.6540	5.0775	5.8087	6.4319	6.4630	6.5858										
^{63}Cu	1.9733	2.2472	2.5229	4.1264	4.8105	5.2484	6.0095	6.6699	6.6959	6.8324	7.1095									
^{73}As	1.9532	2.2315	2.5119	4.1606	4.9179	5.4157	6.2580	7.0086	7.0369	7.1946	7.5246	8.0778								
^{89}Y	1.8952	2.1907	2.4880	4.2394	5.1125	5.7140	6.6929	7.5843	7.6229	7.8085	8.2128	8.9720	10.1862							
^{93}Mo	1.9160	2.2162	2.5181	4.2950	5.1850	5.8006	6.8017	7.7176	7.7558	7.9481	8.3702	9.1671	10.4402	10.7082						
^{120}Sn	1.9196	2.2271	2.5359	4.3670	5.3362	6.0165	7.1132	8.1471	8.1793	8.4078	8.9293	9.9534	11.5807	11.9345	13.7562					
^{124}Sn	1.8959	2.2034	2.5121	4.3449	5.3280	6.0216	7.1351	8.1892	8.2216	8.4553	8.9917	10.0556	11.7447	12.1118	14.0264	14.3119				
^{133}Cs	1.9513	2.2663	2.5824	4.4556	5.4573	6.1637	7.3019	8.3843	8.4138	8.6572	9.2204	10.3329	12.1016	12.4928	14.5770	14.8868	15.5191			
^{153}Gd	1.9216	2.2402	2.5594	4.4485	5.4777	6.2110	7.3864	8.5156	8.5426	8.8008	9.4098	10.6288	12.5719	13.0105	15.4626	15.8287	16.5794	17.9135		
^{184}W	1.6991	1.9925	2.2861	4.0387	5.0556	5.7905	6.9548	8.1022	8.1200	8.3925	9.0554	10.4190	12.5911	13.0945	16.1264	16.5834	17.5174	19.3157	21.5845	
^{208}Pb	1.8500	2.1566	2.4638	4.3069	5.3672	6.1246	7.3340	8.5272	8.5405	8.8276	9.5239	10.9365	13.1860	13.7150	16.9473	17.4319	18.4487	20.4386	23.0338	24.7472

Table 2
Nuclear overlap-like self-similarity measures for the set of 20 nuclei.

Nucleus	Z_{AA}	Nucleus	Z_{AA}	Nucleus	Z_{AA}	Nucleus	Z_{AA}
^{12}C	1.0899	^{40}Ca	4.0662	^{63}Cu	7.1095	^{124}Sn	14.3119
^{14}N	1.2193	^{48}Ca	5.1737	^{73}As	8.0778	^{133}Cs	15.5191
^{16}O	1.3881	^{56}Fe	6.2843	^{89}Y	10.1862	^{153}Gd	17.9135
^{28}Si	2.9426	^{56}Ni	6.3469	^{93}Mo	10.7082	^{184}W	21.5845
^{35}Cl	3.6100	^{58}Ni	6.5858	^{120}Sn	13.7562	^{208}Pb	24.7472

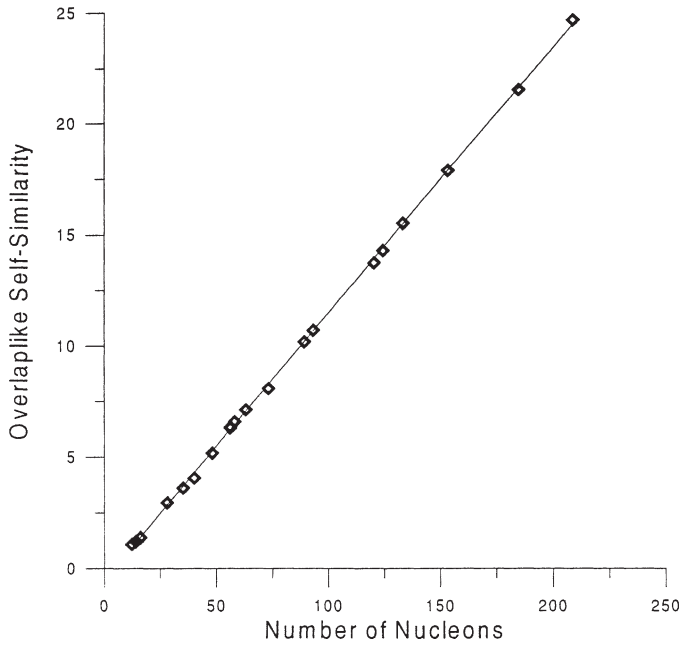

Figure 2. Nuclear overlap-like self-similarities versus massic number. Solid line is a linear regression.

Nuclear SSM are related to the number of nucleons through the equation

$$Z_{\mathrm{AA}} = -0.527 + 0.120A. \tag{5}$$

The negative value of nuclear SSM at the origin can be assigned to the incapability of the Skyrme interaction to give good results for very light nuclei. Forcing the line to go through the origin yields

$$Z_{\mathrm{AA}} = 0.116A. \tag{6}$$

In both cases, the slope of the line is approximately 0.12 fm^{-3}.

From a quantum mechanical point of view, a self-similarity measure is the expectation value of the density operator [13], so it is not surprising that it gives a measure of spatial occupation of matter. In this case, it seems as if nucleons were spread in a constant way as the massic number increases. When a nucleon is added to a given nuclear structure, the self-similarity associated to the system increases approximately by a constant value, denoted by Δ_Z. Thereby, from equations (5) and (6) one can see that the obtained slope is $\Delta_Z \approx 0.12$ fm^{-3}. This value corresponds approximately to the following analytical expression:

$$\Delta_Z = \frac{4}{3}\pi\langle\rho_0\rangle^2, \tag{7}$$

where $\langle\rho_0\rangle$ is the mean value of the nuclear density in the roughly constant range (see figure 1). This expression, however, does not differentiate the isobar nuclei, where

Table 3
Skyrme–HF nuclear radii (in fm) for the studied set.

Nucleus	Radius (fm)	Nucleus	Radius (fm)	Nucleus	Radius (fm)	Nucleus	Radius (fm)
^{12}C	2.42	^{40}Ca	3.40	^{63}Cu	3.81	^{124}Sn	4.73
^{14}N	2.58	^{48}Ca	3.53	^{73}As	4.02	^{133}Cs	4.81
^{16}O	2.62	^{56}Fe	3.67	^{89}Y	4.24	^{153}Gd	5.04
^{28}Si	3.00	^{56}Ni	3.66	^{93}Mo	4.30	^{184}W	5.38
^{35}Cl	3.25	^{58}Ni	3.70	^{120}Sn	4.69	^{208}Pb	5.56

the Coulomb term is overriding. So, Δ_Z will be equal for the studied nuclei ^{56}Fe and ^{56}Ni, whereas the obtained self-similarities are slightly different (6.28 versus 6.35). An analytical approach of the nuclear density function has been used to calculate the SSM integral and put into evidence some trends capable of explaining the linear relationship found. Calculations are given in appendix B.

Remembering that the massic number is the sum of the proton and neutron contributions ($A = Z + N$), the linearity between nuclear SSM and the number of nucleons is straightforwardly translated to the massic number components.

The existing relationship between the nuclear radius and massic number is well known [23]. Approximately, the nuclear radius follows the expression $R = R_0 A^{1/3}$ with $R_0 = 1.23$ fm. The spherical approach of the density functions suggests a definition of a nuclear volume in the usual way, namely,

$$V = \frac{4}{3}\pi R^3 \approx \frac{4}{3}\pi\left(R_0 A^{1/3}\right)^3 = \frac{4}{3}\pi R_0^3 A \propto A. \tag{8}$$

Linear dependence of volume with massic number implies that the linear relationship between nuclear SSM and massic number can be translated to nuclear volume. So, nuclear SSM give an estimation of the size of nucleus. This can be seen in figure 3, where Skyrme–HF values for nuclear radii have been used (given in table 3).

The relationship between nuclear volume and nuclear self-similarities can be written as

$$V_{\text{nuc}} = 36.361 + 27.778 Z_{\text{AA}}. \tag{9}$$

3.2. *Visualization and interpretation of similarity data: Projection of the nuclear cloud*

From this quantum similarity analysis some trends can be put into evidence in order to classify the studied nuclear set. The method used [5,7,9–11,13] is based on the consideration that, for any set of N nuclei, every one of them can be represented by a N-dimensional vector: a column vector of the similarity matrix. The vector components are the similarities of a given nucleus with the N nuclei of the set. This means that every nucleus can be represented as a point in a N-dimensional space, a *point-nucleus*. The closer two point-nuclei are, the more similar will be the nuclei

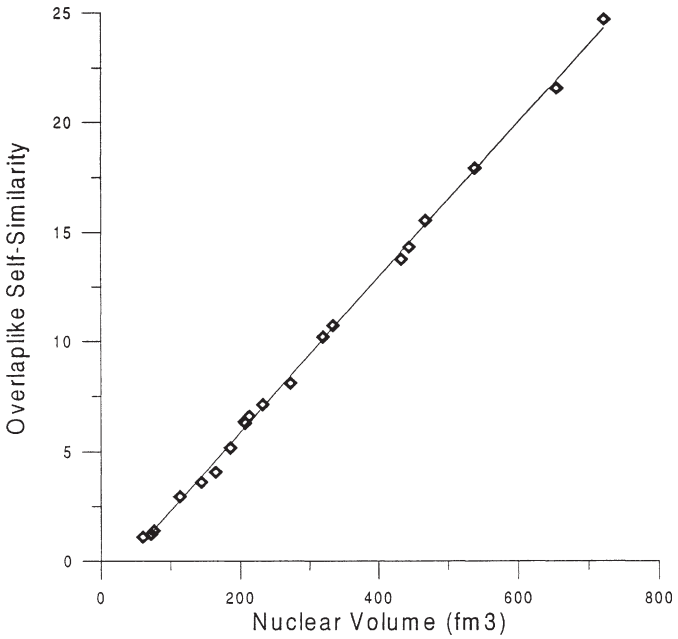

Figure 3. Nuclear overlap-like self-similarities versus nuclear volume. Radii used to calculate nuclear volumes are obtained Skyrme–HF values, not experimental ones. Solid line is the best fit.

they represent. A set of point-nuclei will be called a *nuclear cloud*. Nomenclature has been adapted straightforwardly from the one used in quantum chemistry.

There are many ways to extract information from the QSM and QSI [3,19,22, 35,38]. Among all of them, we have chosen the possibility consisting in making a projection of the nuclear cloud from the original N-dimensional space to any subspace having dimension $M < N$. Then, the *Mendeleev conjecture* can be applied [4,8], which states that by performing different projections an ordering of the different nuclei can be achieved for any property. Thereby, if a projection is found such that it can classify a set of nuclei into groups in relation to a determined known property, one can expect that nuclei with unknown property values will be spatially located in such a way that they will be associated to any of the groups of known nuclei. In that way, a prediction of the property for these unknown nuclei could be done, if not quantitatively, at least qualitatively.

Projection of the nuclear cloud is made as follows. According to a well-known variational principle [37], the eigenvectors of a definite positive matrix **Z** are the optimal space directions where the projections of the objects can be made with a minimal loss of information from the original set. These eigenvectors are also known as the principal components of the matrix. The **Z** matrix canonical decomposition is

$$\widehat{z} = \sum_{i=1}^{N} \lambda_i \widehat{x}_i^{\mathrm{T}} \widehat{x}_i, \tag{10}$$

where λ_i are the eigenvalues (and an order is imposed: $\lambda_1 > \lambda_2 > \cdots > \lambda_N$) of the matrix **Z**, and $\widehat{x}_i$ its eigenvectors. Correlation matrices (and QSM, QSI are that) have the property that they possess a few number of high eigenvalues and a high number of low eigenvalues. This enables to truncate the summation in the first few terms, maintaining a good approximation of the matrix elements. Thus

$$\widehat{z} = \sum_{i=1}^{N} \lambda_i \widehat{x}_i^{\mathrm{T}} \widehat{x}_i \approx \sum_{i=1}^{M} \lambda_i \widehat{x}_i^{\mathrm{T}} \widehat{x}_i \tag{11}$$

with $M < N$. If we choose only two terms, we will be able to perform a bidimensional projection of the nuclear cloud, and making visualizable the set. Once the representation is made, *a posteriori* interpretation of the axes and their association with nuclear properties can be stated.

In the plot, spatial components of each object will be the corresponding components of its eigenvector. So, if the two main principal components of the representation are expressed using columns $(\widehat{a}_1, \widehat{a}_2)$ then the kth point-nucleus will have components (a_{k1}, a_{k2}) in the plane defined by the axes 1 and 2. This study is known as Principal Component Analysis (PCA). A percentage coefficient of explained variation between the objects of the set can be defined as

$$\%\text{ of explained variation} = 100 \sum_i \frac{\lambda_i}{\mathrm{Tr}(\mathbf{Z})}, \tag{12}$$

where Tr(**Z**) is the trace of the matrix **Z**. This coefficient will provide us with an estimation of the loss of information occurred when the reduction of dimensions is achieved.

3.3. Projection of the nuclear cloud generated by the Carbó matrix: Prediction of nuclear ground-state properties

From the QSM matrix elements shown in table 1 and using Carbó Index definition (4), the Carbó matrix has been derived (see table 4). The Carbó matrix elements are nothing but a normalization of similarity measures, performed in order to interpret them more easily. From table 3, one can see that the factor that defines mainly the similarity between two nuclides is, as one could expect, the number of nucleons. So, the closer the massic numbers of two nuclei are, the more similar will be these nuclei. This is an obvious result of the application of this method to a nuclear system (but not so obvious if we were dealing with molecules), and of course, it is not the main result it is expectable to obtain. Quantum similarity enables us to extract much more information from the similarity matrix than a qualitative estimation of the resemblance between nuclei.

With the instructions of the last section, we proceed to perform a projection of the nuclear cloud generated by the Carbó Index matrix. Diagonalization has been made with the Jacobi rotation method [14,21,41], and the eigenvalues of the matrix

Table 4
Quantum similarity measures matrix.

C	^{12}C	^{14}N	^{16}O	^{28}Si	^{35}Cl	^{40}Ca	^{48}Ca	^{56}Fe	^{56}Ni	^{58}Ni	^{63}Cu	^{73}As	^{89}Y	^{93}Mo	^{120}Sn	^{124}Sn	^{133}Cs	^{153}Gd	^{184}W	^{208}Pb
^{12}C	1.0000																			
^{14}N	0.9939	1.0000																		
^{16}O	0.9792	0.9956	1.0000																	
^{28}Si	0.9040	0.9444	0.9698	1.0000																
^{35}Cl	0.8666	0.9101	0.9389	0.9901	1.0000															
^{40}Ca	0.8089	0.8595	0.8950	0.9700	0.9936	1.0000														
^{48}Ca	0.7530	0.8085	0.8488	0.9421	0.9776	0.9951	1.0000													
^{56}Fe	0.7172	0.7735	0.8149	0.9161	0.9604	0.9850	0.9969	1.0000												
^{56}Ni	0.6980	0.7567	0.8004	0.9082	0.9545	0.9817	0.9957	0.9995	1.0000											
^{58}Ni	0.7048	0.7617	0.8037	0.9078	0.9545	0.9812	0.9951	0.9998	0.9996	1.0000										
^{63}Cu	0.7089	0.7632	0.8031	0.9022	0.9496	0.9761	0.9909	0.9979	0.9968	0.9985	1.0000									
^{73}As	0.6583	0.7111	0.7501	0.8534	0.9107	0.9450	0.9680	0.9837	0.9828	0.9864	0.9929	1.0000								
^{89}Y	0.5688	0.6216	0.6617	0.7744	0.8431	0.8879	0.9219	0.9479	0.9481	0.9534	0.9651	0.9891	1.0000							
^{93}Mo	0.5608	0.6133	0.6531	0.7651	0.8340	0.8791	0.9138	0.9408	0.9408	0.9465	0.9593	0.9857	0.9996	1.0000						
^{120}Sn	0.4958	0.5438	0.5803	0.6864	0.7572	0.8045	0.8432	0.8763	0.8754	0.8833	0.9029	0.9442	0.9783	0.9833	1.0000					
^{124}Sn	0.4800	0.5274	0.5636	0.6695	0.7412	0.7894	0.8292	0.8635	0.8626	0.8709	0.8914	0.9352	0.9727	0.9784	0.9997	1.0000				
^{133}Cs	0.4745	0.5210	0.5564	0.6593	0.7291	0.7759	0.8149	0.8490	0.8478	0.8563	0.8778	0.9229	0.9625	0.9691	0.9977	0.9989	1.0000			
^{153}Gd	0.4349	0.4793	0.5133	0.6127	0.6812	0.7277	0.7673	0.8026	0.8012	0.8103	0.8338	0.8836	0.9307	0.9394	0.9850	0.9886	0.9944	1.0000		
^{184}W	0.3503	0.3884	0.4176	0.5068	0.5727	0.6181	0.6581	0.6957	0.6937	0.7039	0.7310	0.7891	0.8492	0.8613	0.9359	0.9435	0.9571	0.9823	1.0000	
^{208}Pb	0.3562	0.3926	0.4204	0.5047	0.5678	0.6105	0.6481	0.6838	0.6815	0.6915	0.7180	0.7735	0.8305	0.8425	0.9185	0.9263	0.9414	0.9707	0.9966	1.0000

Table 5
Eigenvalues of the Carbó Index matrix, ordered decreasingly.

$\lambda_1 = 16.7064$	$\lambda_2 = 2.6060$	$\lambda_3 = 0.5780$	$\lambda_4 = 0.8962 \times 10^{-1}$
$\lambda_5 = 0.1614 \times 10^{-1}$	$\lambda_6 = 0.3436 \times 10^{-2}$	$\lambda_7 = 0.3464 \times 10^{-3}$	$\lambda_8 = 0.4621 \times 10^{-4}$
$\lambda_9 = 0.17237 \times 10^{-4}$	$\lambda_{10} = 0.7587 \times 10^{-5}$	$\lambda_{11} = 0.2961 \times 10^{-5}$	$\lambda_{12} = 0.2452 \times 10^{-5}$
$\lambda_{13} = 0.1845 \times 10^{-5}$	$\lambda_{14} = 0.6534 \times 10^{-6}$	$\lambda_{15} = 0.3276 \times 10^{-7}$	$\lambda_{16} = -0.5334 \times 10^{-7}$
$\lambda_{17} = -0.7599 \times 10^{-6}$	$\lambda_{18} = -0.3586 \times 10^{-5}$	$\lambda_{19} = -0.5451 \times 10^{-5}$	$\lambda_{20} = -0.6056 \times 10^{-5}$

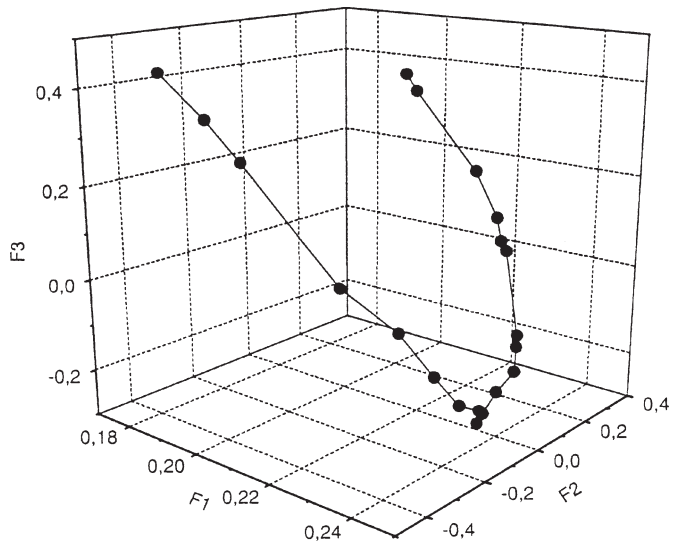

Figure 4. Three-dimensional representation of the nuclear cloud, projected onto the three first principal components, denoted by F1, F2 and F3, respectively.

are shown in table 5. A definite positive matrix cannot have negative eigenvalues, and all that appear are consequence of the approximative nature of the iterative procedure of Jacobi transformation.

From equation (12) and taking into account that the trace of the Carbó matrix is nothing but the cardinality of the system, we determine that the three first eigenvalues contain the 99.5% of the explained variation among nuclei, hence the reduction from the 20-dimensional original space to a 3-dimensional subspace is justified.

Figure 4 shows a 3-dimensional projection of the nuclear cloud. This plot can be thought as a representation of a new type of Nuclear Periodic Table, where positions, relative distances and angles among nuclei are determined by a magnitude related to their internal structure (their density functions), instead of the usual flat classification where the location of a nucleus is determined by its number of protons and neutrons. Hence, from our point of view, construction of a Nuclear Periodic Table where the location of a nucleus depends on a magnitude that contains all its information is a subject of great taxonomic and physical interest. It is to be presumed that an extension of the study to a larger set of nuclei would set the new nuclides following the clear trend shown in figure 4 in relation to their massic number. Furthermore, other representations of the nuclear cloud can be performed using elements of graph theory, and therefore other types of periodic tables can be achieved.

The two first eigenvalues of the Carbó matrix contain the 96.6% of the explained variation among nuclei, hence a bidimensional projection of the set should allow us to extract relevant information of the system. A projection of figure 4 onto the first two principal components (denoted by F1 and F2, respectively) is shown in figure 5.

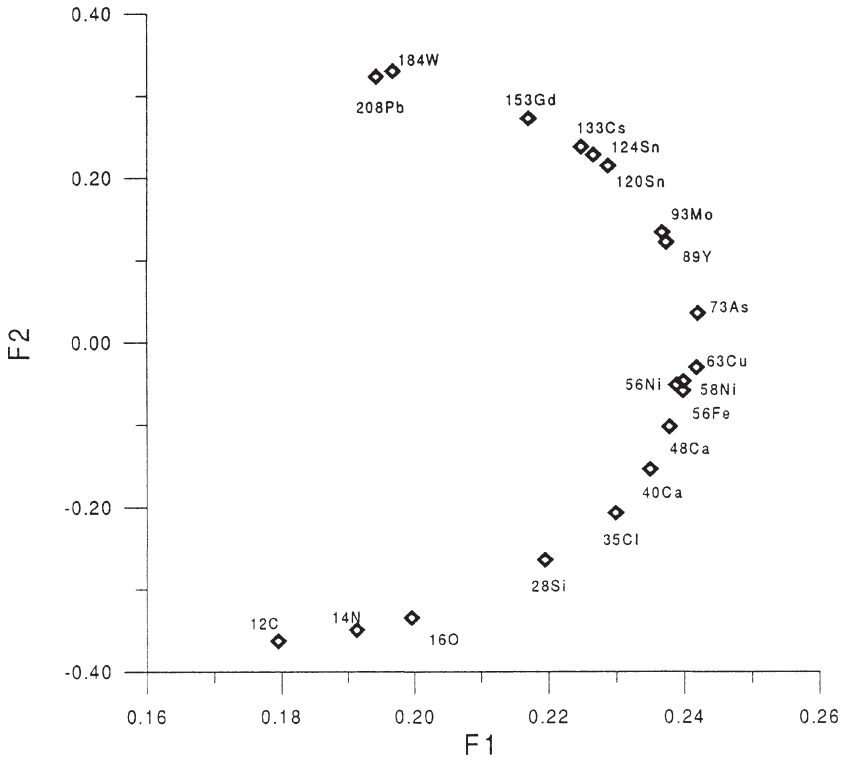

Figure 5. Bidimensional projection of the nuclear cloud onto the two first principal components (denoted by F1, F2). The massic number and the chemical element name of each nucleus label the point-nuclei.

One can see that nuclei follow a "half-moon" distribution trend, ordered decreasingly. Once the projection is performed, relationships between the principal components and nuclear properties can be found.

It can be seen that the first principal component (F1) tends to group extreme nuclei of the set. A basical ground-state nuclear property has tried to be related to it: total binding energy per nucleon. Binding energy per nucleon is of a relatively constant magnitude (except for very light nuclei), with a smooth peak near $A = 56$. This value indicates where nuclei are most tightly bound, so binding energy per nucleon is, somehow, a measure of the stability of a nuclear configuration. In order to state this relationship, a representation of the same plot labelling each point-nucleus with the corresponding value of this magnitude is shown in figure 6. Calculated Skyrme–HF values of this property are given in table 6.

Correlation between both magnitudes can be put into evidence by plotting the projection of the point-nuclei onto the first principal component versus the total binding energy per nucleon. Figure 7 shows this. The first principal component and the total binding energy per nucleon are related through the linear equation

$$\mathrm{F1} = -0.220 - 5.287 \times 10^{-2} \cdot (E/A). \tag{13}$$

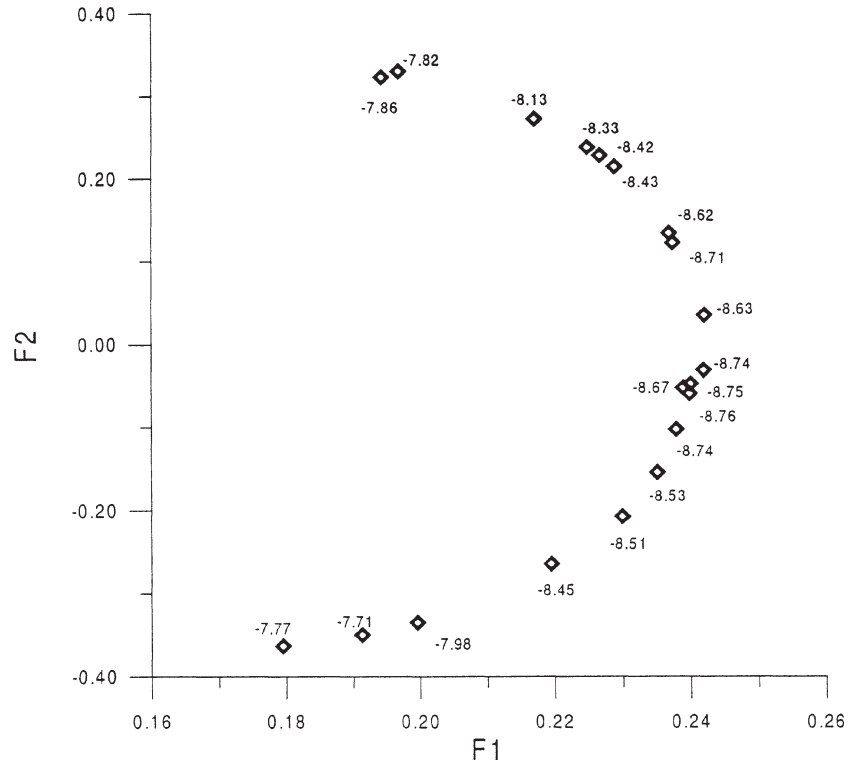

Figure 6. Same plot as figure 5, but labelling each point-nucleus with its calculated value of the total binding energy per nucleon.

Alternatively, the second principal component (F2) values increase with the size of nucleus, thus this axis can be straightforwardly related to size-like properties, such as the number of nucleons, nuclear mass, nuclear radius or nuclear volume. Moreover, there are some ground-state properties that increase with massic number, as total energy or some partial energies (kinetic energy, volume and surface energies, Coulomb energy, etc.). The calculated values of some of these properties are shown in table 6.

Existing relationship between these properties and the number of nucleons make possible to connect them to the second principal component. Some of these relationships are shown in figures 8–14, and can be expressed through the following equations:

$$\text{F2-massic number:} \quad \mathrm{F2} = -0.46 + 8.33 \times 10^{-3} \cdot A - 2.22 \times 10^{-5} \cdot A^2, \tag{14}$$

$$\text{F2-rms radius:} \quad \mathrm{F2} = 0.562 - 1.099r + 0.375r^2 - 0.033r^3, \tag{15}$$

$$\text{F2-volume energy:} \quad \mathrm{F2} = -0.439 - 2.623 \times 10^{-4} \cdot E_{\mathrm{vol}} - 2.256 \times 10^{-8} \cdot (E_{\mathrm{vol}})^2, \tag{16}$$

Table 6
Calculated Skyrme–Hartree–Fock values of energies and nuclear radii for the twenty nuclei.

Nucleus	Kinetic energy (MeV)	Volume energy (MeV)	Surface energy (MeV)	Coulomb energy (MeV)	Total energy (MeV)	E/A (MeV per nucleon)
^{12}C	183.76	−312.83	51.17	8.14	−93.29	−7.77
^{14}N	201.27	−359.51	50.56	10.65	−108.00	−7.71
^{16}O	220.89	−414.43	53.38	13.56	−127.75	−7.98
^{28}Si	484.96	−806.98	92.56	39.08	−236.52	−8.45
^{35}Cl	575.79	−994.19	92.04	54.41	−297.86	−8.51
^{40}Ca	633.13	−1142.73	97.98	72.06	−341.13	−8.53
^{48}Ca	828.22	−1404.38	120.33	71.32	−419.45	−8.74
^{56}Fe	1001.30	−1684.62	136.23	115.49	−490.65	−8.76
^{56}Ni	1008.90	−1704.94	144.99	133.12	−485.46	−8.67
^{58}Ni	1044.72	−1759.92	142.12	132.56	−507.32	−8.75
^{63}Cu	1121.09	−1885.26	136.53	139.74	−550.45	−8.74
^{73}As	1258.65	−2176.50	141.25	172.66	−630.31	−8.63
^{89}Y	1558.98	−2722.41	175.60	229.87	−775.08	−8.71
^{93}Mo	1667.49	−2857.38	178.96	262.82	−801.69	−8.62
^{120}Sn	2137.33	−3653.84	194.87	347.37	−1011.75	−8.43
^{124}Sn	2242.22	−3779.82	203.98	345.54	−1043.65	−8.42
^{133}Cs	2431.12	−4083.92	209.45	410.04	−1107.65	−8.33
^{153}Gd	2791.57	−4723.85	226.24	530.52	−1244.28	−8.13
^{184}W	3426.41	−5710.95	284.65	667.51	−1439.51	−7.82
^{208}Pb	3857.23	−6465.55	281.51	796.68	−1634.88	−7.86

$$\text{F2-surface energy:}\quad \mathrm{F2} = -0.406 - 4.285\times 10^{-4}\cdot E_{\mathrm{surf}} + 3.412\times 10^{-5}\cdot (E_{\mathrm{surf}})^2 - 8.286\times 10^{-8}\cdot (E_{\mathrm{surf}})^3, \tag{17}$$

$$\text{F2-kinetic energy:}\quad \mathrm{F2} = -0.434 + 4.412\times 10^{-4}\cdot E_{\mathrm{kin}} - 6.419\times 10^{-8}\cdot (E_{\mathrm{kin}})^2, \tag{18}$$

$$\text{F2-Coulomb energy:}\quad \mathrm{F2} = -0.368 + 3.130\times 10^{-3}\cdot E_{\mathrm{Coul}} - 5.122\times 10^{-6}\cdot (E_{\mathrm{Coul}})^2 + 2.900\times 10^{-9}\cdot (E_{\mathrm{Coul}})^3, \tag{19}$$

$$\text{F2-total energy:}\quad \mathrm{F2} = -0.456 - 9.610\times 10^{-4}\cdot E_{\mathrm{tot}} - 2.944\times 10^{-7}\cdot (E_{\mathrm{tot}})^2. \tag{20}$$

These results enable us to predict some nuclear ground-state properties. The set could be also projected onto other principal components (eigenvectors of lower eigenvalues), and then try to relate the obtained results to other magnitudes.

Once the projection of a N-particle set is achieved, prediction of any associated property for a new nucleus is easily made: one must calculate the density function of the unknown nucleus, obtain QSM and QSI and project the new set (($N+1$)-particle set) onto the appropriate axes. The nucleus with the unknown property will be set in

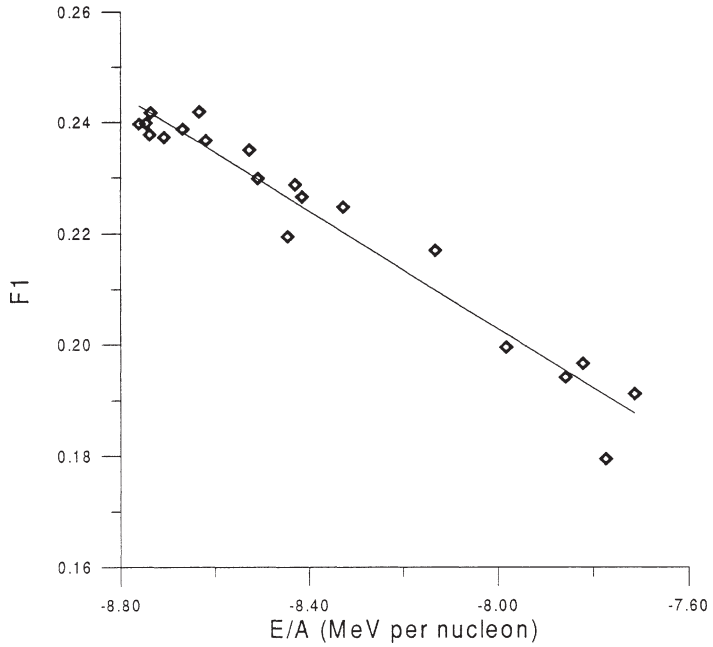

Figure 7. Projection of the nuclear cloud onto the F1-axis versus total binding energy per nucleon. Solid line is a linear fit.

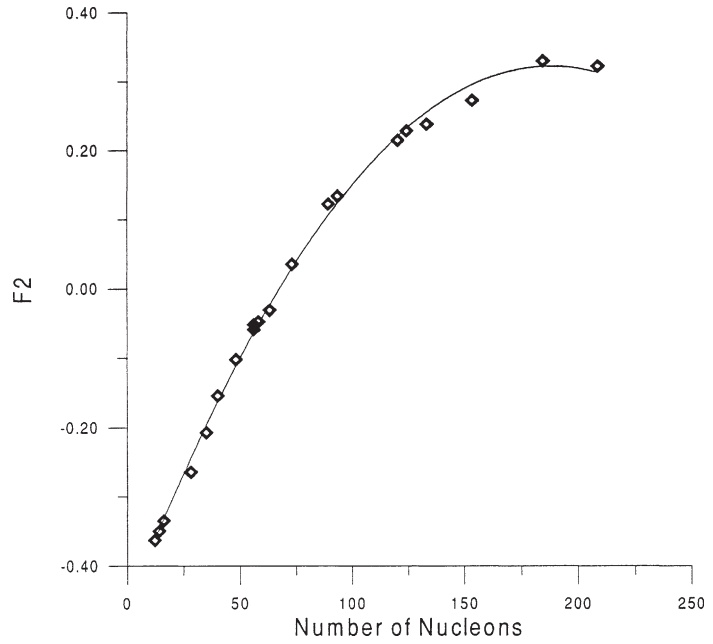

Figure 8. Projection of the nuclear cloud onto F2-axis versus the number of nucleons. Solid line shows a second-degree polynomial fit.

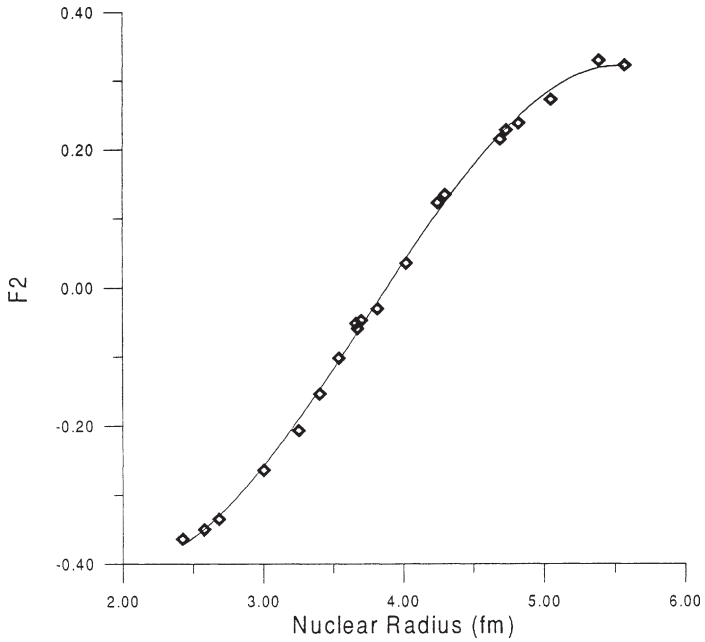

Figure 9. Projection onto the F2-axis versus Skyrme–Hartree–Fock root mean square radius plot. A third-degree polynomial fit is plotted.

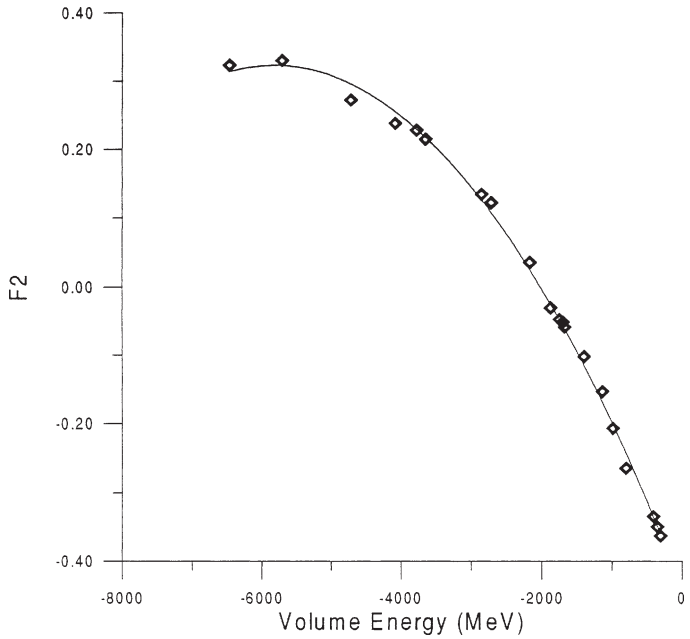

Figure 10. Projection of the nuclear cloud onto the F2-axis versus volume energy. Skyrme–HF values are used. A second-degree polynomial fit is plotted.

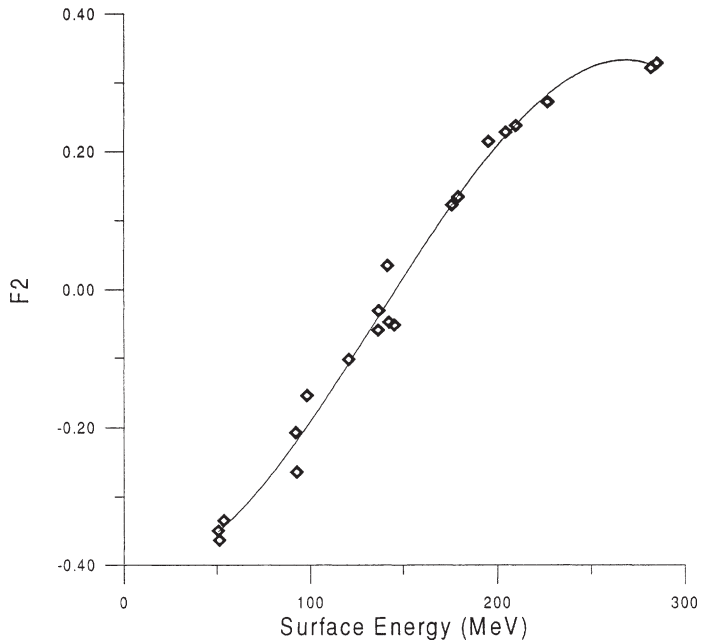

Figure 11. Projection onto the F2-axis versus Skyrme–HF surface energy. A third-degree polynomial fit is plotted.

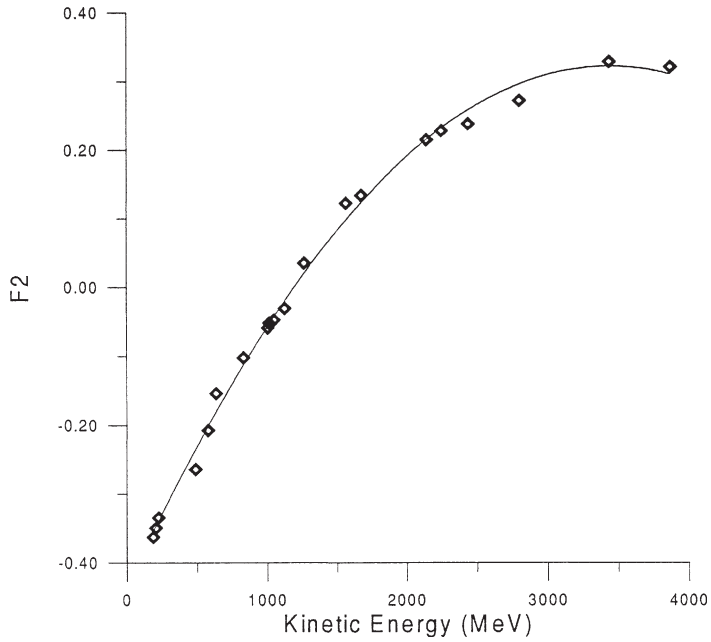

Figure 12. Projection of the nuclear cloud onto the F2-axis versus kinetic energy plot. Solid line shows a second-degree polynomial fit.

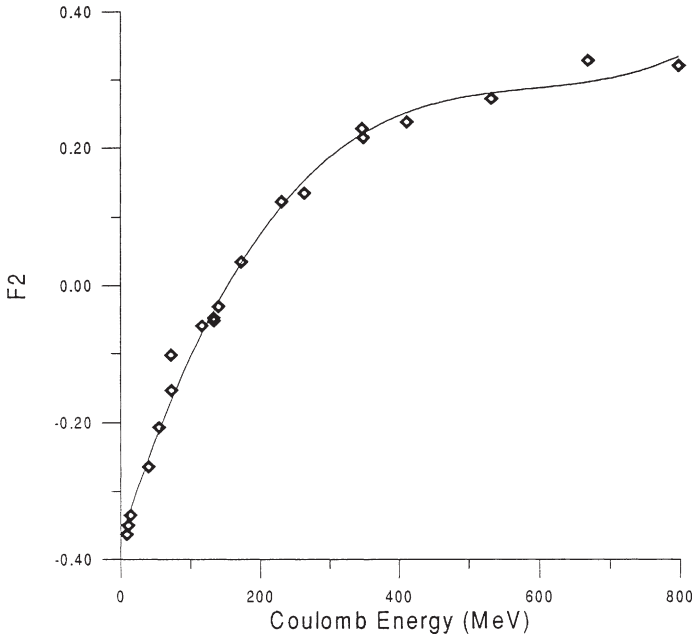

Figure 13. Projection of the nuclear cloud onto the F2-axis versus Skyrme–HF calculated Coulomb energy. A third-degree polynomial fit has been plotted.

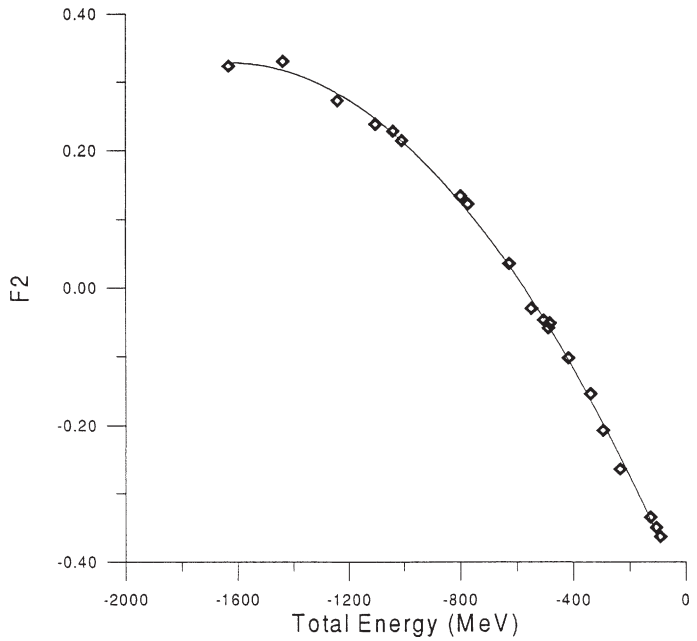

Figure 14. Projection onto the F2-axis versus Skyrme–HF total energy. Solid line shows a second-degree polynomial fit.

a region of that distribution, and that region will be related to an approximated value of the requested property.

In principle, these results do not justify the usefulness of the application of quantum similarity to nuclear systems, since all the properties predicted can be estimated either using existing relationships between them and the massic number or using simple manipulations of the wavefunctions or the density functions. However, remembering the role that quantum mechanical postulates confer on density functions (the contents of all the information of the system), quantum similarity can proportionate us an estimation of the values of certain magnitudes that cannot be obtained by manipulating mathematically the nuclear wavefunctions. We are referring, for instance, to properties related to nuclear stability: qualitative prediction of mean lifetime or mode decay of a radiactive nuclide could be estimated with this technique. In any case, these results state the fact that quantum similarity is able to extract relevant information from the nuclear density functions.

4. Conclusions

This work constitutes, using atomic nuclei, the first attempt to extend quantum similarity to other areas dealing with quantum objects different from molecules.

In order to establish a formal comparison between the different elements of a nuclear system, nuclear quantum similarity measures and indices have been defined analogously to molecular ones. A study of the similarity data obtained with these magnitudes has allowed us to come to the following conclusions: first, nuclear quantum self-similarities give a measure of the comparison between identical nuclei. We have seen that this magnitude gives an estimation of size of nuclei, and of how nucleons are spread in space. A linear relationship between them and size-like properties (massic number and nuclear volume) is found.

Projection of the nuclear cloud from the original 20-dimensional space to a 2-dimensional subspace has been performed in order to extract information from the similarity data. A PCA has been performed taking as axes of the representations the two first principal components of the Carbó matrix. This study associates the axes with nuclear ground-state properties such as total binding energy per nucleon, total or partial energies, and root mean square radius. In the same manner, lower principal components could be taken as axes of new representations. After that, relationships between these new axes and other nuclear properties could be searched.

Zermelo's theorem [17] and the Mendeleev conjecture are some of the theoretical bases of this study. These principles, together with the different techniques of visualization, also provide a way to construct a new type of Nuclear Periodic Table: a bidimensional or three-dimensional periodic table where positions, relative distances and angles between nuclei are related to the foundations of their quantum structure – their respective density functions.

However, there are several degrees of freedom in the present study. A Dirac delta function has been chosen here to be the operator of the QSM integrals, but obviously it

is not the only possible choice. Other operators frequently used in molecular physics are a Coulomb operator ($\Omega(\mathbf{r}_1, \mathbf{r}_2) = 1/r_{12}$) [5,7,9–11,13], a gravitational operator ($\Omega(\mathbf{r}_1, \mathbf{r}_2) = 1/r_{12}^2$) [4], or another density function (thus, using the so-called triple-density similarity measures) [12]. Further, other similarity indices can be used, as the Distance Dissimilarity Index [7], the Hodgkin–Richards [20] or Tanimoto [38] Indices, or the Petke Index [31]. Last, other visualization techniques can be used in order to interpret the similarity data [3,19,22,35,38]. All these circumstances make our paper a preliminary work in this field, susceptible to be extended and improved in a considerable way.

Finally, this work tries to constitute a first step towards a new point of view in the study of nuclear systems. Further, foundations of quantum similarity make it extensible to other systems, provided they are described in a quantum mechanical way, namely, by a wavefunction, and in extension, by a density function. In this manner, this paper settles the bases for the application of quantum similarity to systems of physical interest such as infinite nuclear matter (quantum similarity in momentum-space has already been discussed [1]), nuclear molecules or atomic systems, among others.

Appendix A. The Skyrme–Hartree–Fock model for the nuclear ground state

So far the exact nature of the relationship between the observed single-particle properties of nuclei and the nucleon–nucleon force has not been resolved. There does not exist, therefore, a realistic method that can describe at the same time the average nucleonic properties (binding energy, nuclear radii, density distributions, etc.) and the excited states in each nucleus. To solve this problem another type of calculations, namely Hartree–Fock calculations with effective interactions, are used. The approach consisting of a direct parametrization of the effective force is obviously less fundamental than using a realistic interaction, but nevertheless has a certain number of advantages, among them a greater precision of the predicted results. Among all the effective interactions proposed, the one presented by T.H.R. Skyrme 38 years ago [34,40] still today continues to be the best tool to describe the ground-state of spherical nuclei. This is the interaction that we have used to obtain the nuclear density functions necessary to the quantum similarity analysis.

Skyrme force is an effective density-dependent interaction with a short-range two-body term and a three-body term:

$$V_{\text{Skyrme}} = \sum_{i<j} V_{ij}^{(2)} + \sum_{i<j<k} V_{ijk}^{(3)}. \tag{21}$$

Explicitly, it can be written as

$$V_{\text{Skyrme}} = t_0(1 + x_0 P_x)\delta(\mathbf{r}_i - \mathbf{r}_j) + \frac{1}{2} t_1(1 + x_1 P_x)\{\mathbf{p}_{12}^2 \delta(\mathbf{r}_i - \mathbf{r}_j) + \delta(\mathbf{r}_i - \mathbf{r}_j)\mathbf{p}_{12}^2\}$$

$$+ t_2(1 + x_2 P_x)\mathbf{p}_{12} \cdot \delta(\mathbf{r}_i - \mathbf{r}_j)\mathbf{p}_{12} + \frac{1}{6} t_3 (1 + x_3 P_x)\rho^{\alpha}\left(\frac{\mathbf{r}_i + \mathbf{r}_j}{2}\right)\delta(\mathbf{r}_i - \mathbf{r}_j)$$
$$+ \mathrm{i} t_4 \mathbf{p}_{12} \cdot \delta(\mathbf{r}_i - \mathbf{r}_j)(\boldsymbol{\sigma}_i + \boldsymbol{\sigma}_j) \cdot \mathbf{p}_{12}, \tag{22}$$

where $\mathbf{p}_{12} = \mathbf{p}_1 - \mathbf{p}_2$ is the relative momentum, P_x is the exchange spin operator and σ are the Pauli matrices. The potential depends on a few parameters: t_0, t_1, t_2, t_3, t_4, x_0, x_1, x_2, x_3, α. These parameters are related to magnitudes as nuclear matter incompressibility or Fermi momentum, and they are fitted to nuclear single-particle properties (binding energies per nucleon, nuclear radii, etc.) [18]. Among the several existing parametrizations, we have used the SkM* [2], given in table 7.

The simplicity of the ansatz makes possible to express the energy functional $H(\mathbf{r})$ as a function of a few densities: density of nucleons, $\rho(\mathbf{r})$, kinetic energy, $\tau(\mathbf{r})$, spin density, $\mathbf{J}(\mathbf{r})$, and the divergence of the spin density, $\nabla \cdot \mathbf{J}(\mathbf{r})$, defined as

$$\begin{aligned}
\rho_q(\mathbf{r}) &= \sum_{\beta \in q} w_\beta \varphi_\beta^+(\mathbf{r})\varphi_\beta(\mathbf{r}), \\
\mathbf{j}_q(\mathbf{r}) &= \frac{\mathrm{i}}{2} \sum_{\beta \in q} w_\beta \left[\nabla \varphi_\beta^+(\mathbf{r})\varphi_\beta(\mathbf{r}) - \varphi_\beta^+ \nabla \varphi_\beta(\mathbf{r})\right], \\
\tau_q(\mathbf{r}) &= \sum_{\beta \in q} w_\beta \nabla \varphi_\beta^+(\mathbf{r}) \nabla \varphi_\beta(\mathbf{r}), \\
\boldsymbol{\nabla} \mathbf{J}_q(\mathbf{r}) &= -\mathrm{i} \sum_{\beta \in q} w_\beta \nabla \varphi_\beta^+(\mathbf{r}) \nabla \times \boldsymbol{\sigma} \varphi_\beta(\mathbf{r}),
\end{aligned} \tag{23}$$

where φ_β is the single-particle wavefunction of the state β and q is the isospin label (protons/neutrons). For doubly closed shell nuclei, spherical symmetry reduces densities position dependence (3 variables) into a radial coordinate dependence (1 variable).

Nonmagic nuclei have been dealt with HF+BCS equations, introducing a weight w_β in the density definitions, interpreted as the ocupation probability of the state β. This factor is obtained through a simple pairing scheme [39].

Radial densities can be written as

$$\begin{aligned}
\rho_q(r) &= \sum_{n_\beta j_\beta l_\beta} w_\beta \frac{2j_\beta + 1}{4\pi} \left(\frac{R_\beta}{r}\right)^2, \\
\tau_q(r) &= \sum_{n_\beta j_\beta l_\beta} w_\beta \frac{2j_\beta + 1}{4\pi} \left[\left(\partial_r \frac{R_\beta}{r}\right)^2 + \frac{l(l+1)}{r^2}\left(\frac{R_\beta}{r}\right)^2\right], \\
\nabla J_q(r) &= \left(\partial_r + \frac{2}{r}\right) J_q(r), \\
J_q(r) &= \sum_{n_\beta j_\beta l_\beta} w_\beta \frac{2j_\beta + 1}{4\pi} \left[j_\beta(j_\beta + 1) - l_\beta(l_\beta + 1) - \frac{3}{4}\right] \frac{2}{r} \left(\frac{R_\beta}{r}\right)^2.
\end{aligned} \tag{24}$$

Table 7
Parameters of the SkM* Skyrme force.

t_0 (MeV fm^3)	t_1 (MeV fm^5)	t_2 (MeV fm^5)	t_3 (MeV fm^6)	t_4 (MeV fm^5)
−2645.0	410.0	−135.0	15595.0	130
x_0	x_1	x_2	x_3	α
0.09	0.0	0.0	0.0	1/6

Once defined the Skyrme potential, the Hartree–Fock equations are obtained by imposing the total energy E to be stationary with respect to the individual variations of the single-particle states, under the constraint that the wavefunctions be orthonormal. The Hartree–Fock equations for the radial wavefunctions R_β are

$$h_\beta R_\beta = \varepsilon_\beta R_\beta \tag{25}$$

with the mean-field Hamiltonian

$$h_q = \partial_r B_q \partial_r + U_q + U_{ls,q}\mathbf{l}\cdot\boldsymbol{\sigma}, \tag{26}$$

where

$$B_q = \frac{\hbar^2}{2m} + \frac{1}{8}\left[t_1\left(1+\frac{1}{2}x_1\right)+t_2\left(1+\frac{1}{2}x_2\right)\right]\rho - \frac{1}{8}\left[t_1\left(\frac{1}{2}+x_1\right)-t_2\left(\frac{1}{2}+x_2\right)\right]\rho_q, \tag{27}$$

$$\begin{aligned} U_q = {} & t_0\left(1+\frac{1}{2}x_0\right)\rho - t_0\left(\frac{1}{2}+x_0\right)\rho_q + \frac{1}{12}t_3\rho^\alpha\left[(2+\alpha)\left(1+\frac{1}{2}x_3\right)\rho\right. \\ & \left. - 2\left(\frac{1}{2}+x_3\right)\rho_q - \alpha\left(\frac{1}{2}+x_3\right)\frac{\rho_{\text{pr}}^2+\rho_{\text{ne}}^2}{\rho}\right] \\ & + \frac{1}{4}\left[t_1\left(1+\frac{1}{2}x_1\right)+t_2\left(1+\frac{1}{2}x_2\right)\right]\tau - \frac{1}{4}\left[t_1\left(\frac{1}{2}+x_1\right)-t_2\left(\frac{1}{2}+x_2\right)\right]\tau_q \\ & - \frac{1}{8}\left[3t_1\left(1+\frac{1}{2}x_1\right)-t_2\left(1+\frac{1}{2}x_2\right)\right]\Delta\rho \\ & + \frac{1}{8}\left[3t_1\left(\frac{1}{2}+x_1\right)+t_2\left(\frac{1}{2}+x_2\right)\right]\Delta\rho_q - \frac{1}{2}t_4(\boldsymbol{\nabla}\mathbf{J}+\boldsymbol{\nabla}\mathbf{J}_q) + U_{\text{Coul}}, \end{aligned} \tag{28}$$

$$U_{ls,q} = \frac{1}{4}t_4(\rho+\rho_q) + \frac{1}{8}(t_1-t_2)J_q - \frac{1}{8}(x_1t_1+x_2t_2)J, \tag{29}$$

where U_{Coul} is the Coulomb contribution.

The mean field localizes the nucleus and breaks translational invariance (and therefore nuclear ground-state is not a state with total momentum zero) [33]. Projecting a state with good total momentum zero out of the given mean-field state is made by modifying the nucleon mass:

$$\frac{\hbar^2}{2m} \to \frac{\hbar^2}{2m}\left(1-\frac{1}{A}\right). \tag{30}$$

Hartree–Fock equations have been solved with the usual iteration procedure. Four point self-consistency in energy has been accomplished using 15 iterations, and a 120-point radial grid has been used. Woods–Saxon potential [24] solutions constitute trial wavefunctions (zero-order) to start the Hartree–Fock iteration. Throughout the calculations proton and neutron masses have been considered equal.

Appendix B. Determination of the linear relationship between nuclear self-similarity measures and the number of nucleons using an analytical approach of the nuclear density function

The objective is to compute the self-similarity integral

$$Z_{\mathrm{AA}} = \int_0^\infty \rho_{\mathrm{A}}^2(r) 4\pi r^2 \, \mathrm{d}r \tag{31}$$

to determine a trend in order to explain the linear relationship between Z_{AA} and the number of nucleons A obtained earlier.

Intuitively, one can expect a linear relationship between both magnitudes because of the shape of the nuclear density functions. Approximately, nuclear densities can be considered as Fermi–Dirac distributions. It is easy to see that these functions are very similar to their squared form, except that they decrease faster. Therefore, integral (31) is essentially identical to the normalization integral, but in the presence of a numerical factor.

We will derive the relationship in a more formal way. In order to do this, we will use a simple analytical approach of the nuclear density functions: the Fermi–Dirac distribution-like density [29,32] given by the equation

$$\rho(r) = \rho_0 \frac{1}{1 + \mathrm{e}^{(r-c)/a}}, \tag{32}$$

where the parameters are defined as

$$\rho_0 = \frac{3A}{4\pi c^3 (1 + \pi^2 a^2 / c^2)}, \tag{33}$$

$$a = 0.54 \text{ fm}, \tag{34}$$

$$c = \left(0.978 + 0.0206 A^{1/3}\right) A^{1/3} \text{ fm}. \tag{35}$$

In the range of studied nuclei ($A = 12$–208) some additional approaches can be made: ρ_0 can be considered roughly constant (and with a mean value of 0.17 fm^{-3}), and the parameter c can be approximated to $c = A^{1/3}$ fm making an error at most of 11%. All these approximations simplify the calculation without introducing a considerable error, and the resulting analytical density function remains a good enough model.

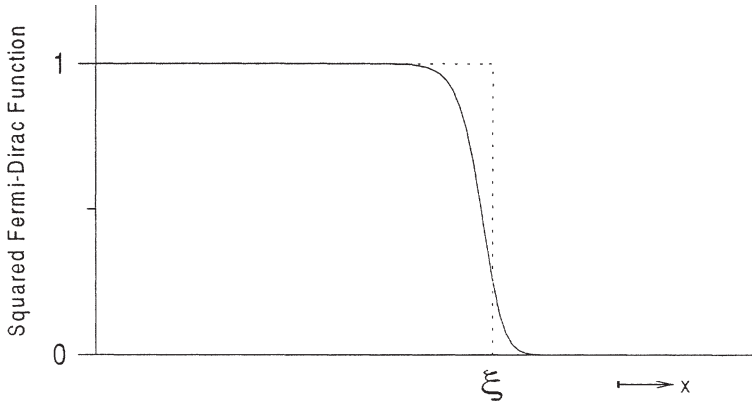

Figure 15. Squared Fermi–Dirac function plot. Dashed line shows the step function.

Then, the integral one wants to solve is

$$Z_{\mathrm{AA}} = 4\pi\rho_0^2 \int_0^\infty r^2 \left(1 + \mathrm{e}^{(r-c)/a}\right)^{-2} \mathrm{d}r. \tag{36}$$

A change of variable is performed to simplify the integral:

$$\frac{r}{a} \equiv x \quad \text{and} \quad \frac{c}{a} \equiv \xi. \tag{37}$$

Introducing this change into equation (37) yields

$$Z_{\mathrm{AA}} = 4\pi\rho_0^2 a^3 \int_0^\infty \frac{x^2}{(1 + \mathrm{e}^{x-\xi})^2} \mathrm{d}x. \tag{38}$$

This integral is hard to solve, so a study of the behaviour of the function along the effective range of integration must be made in order to perform other simplifications. For large values of ξ, the situation is primarily controlled by the factor $(1 + \mathrm{e}^{x-\xi})^{-2}$ (that we will call the squared Fermi–Dirac function), whose departure from its limiting values, namely zero (as $x \to \infty$) and almost unity (as $x \to 0$), is significant only in the neighborhood of the point $x = \xi$. The width of this "region of significance" is much smaller than the total effective range of integration. Therefore, in the lowest approximation, one may replace the actual curve by a step function [30]. This is shown in figure 15.

Equation (38) then reduces to

$$Z_{\mathrm{AA}} \approx 4\pi\rho_0^2 a^3 \int_0^\xi x^2 \,\mathrm{d}x = 4\pi\rho_0^2 a^3 \frac{\xi^3}{3}. \tag{39}$$

Undoing the change of variable, and using the approximations $c \approx A^{1/3}$ and $\rho_0 \approx 0.17$ fm^{-3}, we obtain

$$Z_{\mathrm{AA}} = 4\pi\rho_0^2 a^3 \frac{1}{3}\left(\frac{c}{a}\right)^3 = \frac{4}{3}\pi\rho_0^2 c^3 = \frac{4}{3}\pi\rho_0^2 \left(A^{1/3}\right)^3 \approx 0.12A. \tag{40}$$

This result explains the linear relationship between nuclear SSM and the number of nucleons obtained in section 3.1. The slope of the line also surprisingly agrees, despite the approximations made.

Acknowledgements

This work has been partially sponsored by the project SAF 96-0158 of the CICYT. We would like to thank Dr. Artur Polls (University of Barcelona) for providing us the software performing Skyrme–Hartree–Fock calculations used in this work.

References

[1] N.L. Allan and D. Cooper, in: *Topics in Current Chemistry*, ed. K. Sen (Springer, Berlin, 1995).
[2] J. Bartel, P. Quentin, M. Brack, C. Guet and H.-B. Hakansson, Nucl. Phys. A 386 (1982) 79.
[3] J.-P. Barthélemy and A. Guénoche, *Trees and Proximity Representations* (Wiley, New York, 1991).
[4] E. Besalú and R. Carbó, in: *Topics in Quantum Chemistry*, ed. K. Sen (Springer, Berlin, 1995).
[5] E. Besalú, R. Carbó, J. Mestres and M. Solà, in: *Topics in Current Chemistry*, ed. K. Sen (Springer, Berlin, 1995).
[6] R.L. Burden and J.D. Fayres, *Análisis Numérico* (Grupo Ed. Iberoamericana, 1985).
[7] R. Carbó, J. Arnau and L. Leyda, Int. J. Quantum Chem. 17 (1980) 1185.
[8] R. Carbó and E. Besalú, in: *Molecular Similarity and Reactivity: From Quantum Chemical to Phenomenological Approaches*, ed. R. Carbó (Kluwer, Dordrecht, 1995).
[9] R. Carbó, E. Besalú, B. Calabuig and L. Vera, Adv. Quantum Chem. 25 (1994) 253.
[10] R. Carbó and B. Calabuig, in: *Concepts and Applications of Molecular Similarity*, eds. M.A. Johnson and G.M. Maggiora (Wiley, New York, 1990) p. 147.
[11] R. Carbó and B. Calabuig, Int. J. Quantum Chem. 42 (1992) 1681.
[12] R. Carbó, B. Calabuig, E. Besalú and A. Martínez, Molec. Eng. 2 (1992) 43.
[13] R. Carbó and L. Domingo, Int. J. Quantum Chem. 23 (1987) 517.
[14] R. Carbó, Ll. Molino and B. Calabuig, J. Comput. Chem. 13 (1992) 155.
[15] J.M. Cavendon, Thesis, University of Paris (Orsay) (1980).
[16] B. Dreher, J. Friedrich, K. Merle, H. Rothaas and G. Lührs, Nucl. Phys. A 235 (1977) 219.
[17] *Encyclopaedia of Mathematics* (Kluwer, Dordrecht, 1990).
[18] J. Friedrich and P.-G. Reinhard, Phys. Rev. C 33 (1986) 335.
[19] J.A. Hardigan, *Clustering Algorythms* (Wiley, New York, 1975).
[20] E.E. Hodgkin and W.G. Richards, Int. J. Quantum Chem. 14 (1987) 105.
[21] C.G.J. Jacobi and J. Reine, Angew. Math. 30 (1846) 51.
[22] N. Jardine and R. Sibson, *Mathematical Taxonomy* (Wiley, New York, 1977).
[23] K.S. Krane, *Introductory Nuclear Physics* (Wiley, New York, 1988).
[24] R.D. Lawson, *Theory of the Nuclear Shell Model* (Oxford University Press, New York, 1980).
[25] P.-O. Löwdin, Phys. Rev. 97 (1955) 1474, 1490.
[26] R. McWeeny, Proc. Roy. Soc. London Ser. A 235 (1955) 496.
[27] R. McWeeny, Proc. Roy. Soc. London Ser. A 237 (1955) 355.
[28] R. McWeeny, Rev. Mod. Phys. 32 (1960) 335.
[29] J.W. Negele, Phys. Rev. Lett. C 1 (1970) 1260.
[30] R.K. Pathria, *Statistical Mechanics* (Pergamon Press, Oxford, 1972).
[31] J.D. Petke, J. Comput. Chem. 14 (1993) 928.
[32] M.A. Preston, *Physics of the Nucleus* (Addison-Wesley, Reading, MA, 1962).
[33] P. Ring and P. Schuck, *The Nuclear Many Body Problem* (Springer, Berlin, 1980).

[34] T.H.R. Skyrme, Nucl. Phys. 9 (1959) 615.
[35] P.H.A. Sneath and R.R. Sokal, *Numerical Taxonomy* (Freeman, San Francisco, CA, 1973).
[36] M. Solà, J. Mestres, J.M. Oliva, M. Duran and R. Carbó, Int. J. Quantum Chem. 58 (1996) 361.
[37] M.S. Srivastava and E.M. Carter, *An Introduction to Applied Multivariate Statistics* (Elsevier, New York, 1983).
[38] J.T. Tou and R.C. Gonzalez, *Pattern Recognition Principles* (Addison-Wesley, Reading, MA, 1974).
[39] D. Vautherin, Phys. Rev. C 7 (1973) 296.
[40] D. Vautherin and D.M. Brink, Phys. Rev. C 5 (1972) 626.
[41] J.H. Wilkinson, *The Algebraic Eigenvalue Problem* (Clarendon Press, Oxford, 1965).